# Investigating thermal stability, mechanical and thermal properties for Si/Ge core-shell nanowires at atomic scale

**zhao dandan**
Northeastern University
**Yang Cui**
Northeastern University
**jing li**
Northeastern University
**Naipeng Sun**
Northeastern University
**Lin Zhang** ( zhanglin@imp.neu.edu.cn )
Northeastern University

**Article**

**Keywords:** Si/Ge, Core-Shell Nanowires, MD simulations, Mechanical properties, Thermal properties

**Posted Date:** May 27th, 2022

**DOI:** https://doi.org/10.21203/rs.3.rs-1669431/v1

# Abstract

Molecular dynamics simulations using Tersoff potential are performed to study the structure, atomic pressure and mechanical properties as well as thermal properties for Si/Ge core-shell nanowires with different core-shell ratios at different temperatures. Potential energy and pair distribution functions indicate structural features of these nanowires at different temperatures. During uniaxial tensile along the wire axis at different temperature, different stages including elasticity, plasticity, necking, and fracture are characterized through stress-strain curves, Young's modulus and tensile strength are obtained. The simulation results indicate that as the temperature increases, the elasticity during the stretching process becomes less apparent. The Young's modulus of the Ge@Si and Si@Ge nanowires at room temperature show differences with changing the core-shell ratio. In addition, the atomic level pressures show the differences of these atoms under compression or tension, and the temperature and strain significantly affect the pressure distribution in these wires. Phonon density of states with varying the composition and strain suggest different vibration modes at room temperature, and then the heat capacities of these nanowires are determined.


# 1 Introduction

Semiconductor nanowires with modulated compositions, such as core-shell nanowires, have received extended interests due to their enhanced thermal and mechanical properties compared to their bulk counterparts[1–5]. In the past decade, Si/Ge core-shell nanowires, which could be easily integrated with the current Si-based technology [6–10], have attracted more attention both experimentally and theoretically[11–13]. It is worth noting that the structural changes can significantly affect the mechanical and thermal properties of Si/Ge-based materials, which are of great importance for further application for these core–shell nanowires.

Tensile test[14] has been an effective approach to probe the mechanical properties. However, unlike the mechanical testing of bulk materials, the testing of nanowires heavily depends on the experimental setup so that there are significant challenges during manipulating, which makes accurately applying and measuring the external force or strains at the nano-scale be hardly possible. Therefore, computational approaches have been used to calculate the mechanical properties of reasonably sized nanowires. Many tensile investigations for some core-shell nanowires has been reported[15–17]. For example, Liu et al.[18] has been studied the composition-dependent stiffness for Ge-core/Si-shell and Si-core/Ge-shell nanowires using Stillinger–Weber potential. The results revealed that the trends of Young's modulus of core–shell nanowires are essentially attributed to the different components of the cores and the shells. Then, Thanh et al.[19] used the molecular dynamics (MD) method to investigate the mechanical properties of Si/Ge and Ge/Si NWs under the axial tensile strain and further researched the effect of different strain rate on the mechanical properties of these materials. However, the stress distribution at atomic scale has not been presented to show the loading states on the atoms under the effect of the temperature and applied external force.

Besides the mechanical properties being related to the packing structures, the design of effective application also requires characteristics of thermal properties, which can be determined from lattice vibrational modes, such as the heat capacity ($C_V$). Previous studies have found that heat capacity varies with size, temperature and the structure of different modulated composition. Zhu et al. [20]discussed the heat capacity as a function of temperature of order and disorder phases of $Si_xGe_{1-x}$ alloys through the quasi-harmonic Debye model. Zhang et al.[21] have investigated the specific heat of silicon nanowires with Stillinger-Weber potential. It is found that the specific heats of thin nanowires are much higher than those of bulk silicon and the enhancement of specific heats of silicon nanowires can be attributed to the surface effect and phonon confinement effect. As far as known, introducing strain has a significant affluence to materials properties[21–27]. Therefore, understanding the thermal response of materials from applied external strain is not overemphasized.

In this paper, Si@Ge and Ge@Si nanowires different core-shell ratios have been compared to investigate the structural stability at elevated temperature via potential energy and pair distribution function from molecular dynamics simulations. The mechanical properties under tension for these nanowires are studied at different temperatures, including the stress-strain curves, tensile strength and Young's modulus as well as atomic level stress. Phonons' density of states is used for calculating the heat capacities for the nanowires having different core-shell ratios at room temperature.

# 2 Simulation Detail

In MD simulations performed herein, the Tersoff potential was used to describe the Si − Si, Ge − Ge, and Si − Ge interactions in the present Si/Ge NWs. This potential[28] has been widely used to predict the molecular structure and the thermal properties of Si/Ge nanomaterials[29].

As a function of atomic coordinates, the total potential energy $E$ takes the following forms:

$$E_{tot} = \frac{1}{2}\sum_{i \neq j} V_{ij}$$

1

$$V_{ij} = f_C\left(r_{ij}\right)\left[f_R\left(r_{ij}\right) + b_{ij}f_A\left(r_{ij}\right)\right]$$

2

$$f_R\left(r_{ij}\right) = A_{ij}\exp\left(-\lambda_{ij}r_{ij}\right)$$

3

$$f_A\left(r_{ij}\right) = -B_{ij}\exp\left(-\mu_{ij}r_{ij}\right)$$

4

$$f_C\left(r_{ij}\right)=\begin{cases}1, r_{ij}<R_{ij}\\ \frac{1}{2}+\frac{1}{2}\cos\frac{\pi\left(r_{ij}-R_{ij}\right)}{S_{ij}-R_{ij}}, R_{ij}<r_{ij}<S_{ij}\\ 0, r_{ij}>S_{ij}\end{cases}$$

5

$$b_{ij}=\chi_{ij}\left(1+\beta_i^{n_i}\zeta_{ij}^{n_i}\right)^{-\frac{1}{2n_i}}$$

6

$$\zeta_{ij}=\sum_{k\neq i,j}f_C\left(r_{ik}\right)\omega_{ik}g\left(\theta_{ijk}\right)$$

7

$$g\left(\theta_{ijk}\right)=1+\frac{{c_i}^2}{{d_i}^2}-\frac{{c_i}^2}{{d_i}^2+\left(h_i+\cos\theta_{ijk}\right)^2}$$

8

$$\lambda_{ij}=\frac{\lambda_i+\lambda_j}{2},\ \mu_{ij}=\frac{\mu_i+\mu_j}{2}$$

$$A_{ij}=\left(A_iA_j\right)^{\frac{1}{2}},\ B_{ij}=\left(B_iB_j\right)^{\frac{1}{2}},\ R_{ij}=\left(R_iR_j\right)^{\frac{1}{2}},\ S_{ij}=\left(S_iS_j\right)^{\frac{1}{2}}$$

9

where $V_{ij}$is the bond energy between ij atoms, $f_R$ and $f_A$ are attractive and repulsive terms of the potential, $f_C$ refers to the slip cutoff function, and $b_{ij}$ is the key sequence function. $r_{ij}$is the length of the $ij$ bond, and $\theta_{ijk}$ is the bond angle between bonds $ij$and$ik$. The crucial parameters are listed in Table 1.

Table 1
Parameters for silicon and germanium to be used.

| Parameter | Si | Ge |
|---|---|---|
| A (eV) | $1.8308\times10^{3}$ | $1.769\times10^{3}$ |
| B (eV) | $4.7118\times10^{2}$ | $4.1923\times10^{2}$ |
| λ(Å$^{-1}$) | 2.4799 | 2.4551 |
| μ(Å$^{-1}$) | 1.7322 | 1.7047 |
| β | $1.1000\times10^{-6}$ | $9.0166\times10^{-7}$ |
| n | $7.8734\times10^{-1}$ | $7.5627\times10^{-1}$ |
| c | $1.0039\times10^{5}$ | $1.0643\times10^{5}$ |
| d | $1.6217\times10^{1}$ | $1.5652\times10^{1}$ |
| h | $-5.9825\times10^{-1}$ | $-4.3884\times10^{-1}$ |
| R (Å) | 2.7 | 2.8 |
| S (Å) | 3.0 | 3.1 |
| $\chi_{Si-Ge}$=1.00061 | | |

Initially, after directly cleaving from bulk silicon, one silicon nanowire including 2080 atoms along the ⟨110⟩ direction was built with exposing the (100) and (111) surfaces due to the fact that experimental studies have reported the ⟨110⟩ as the preferred growth direction for a diameter less than 20 nm[30–32]. After constructing the silicon nanowires, the Ge core or shell segments were built by replacing Si atoms with Ge. Therefore, the Si@Ge nanowires with different composition are the ones with the Ge atoms in the core and Si in the shell. Analogously, the Ge@Si nanowires with different composition have a core of Si and a shell of Ge. The structures of the Si@Ge and Ge@Si nanowires are shown in Fig. 1, where the yellow balls represent silicon and green balls is germanium atoms, respectively. The structural parameters are listed in Table 2.

To ensure a negligible interaction between the nanowires from its periodic images, we created a supercell with a lattice parameter of 100 Å in the x- and y- directions to ensure the isolation of the nanowires. The periodic boundary condition along z direction is considered to have infinite length in this direction. The open visualization tool OVITO[33] was used to identify structural changes.

Table 2
The structural parameters of Ge@Si and Si@Ge nanowires with different core-shell ratios

| Type | Side length of shell (nm) | | Label | Ge% | Side length of core (nm) | |
|---|---|---|---|---|---|---|
| | a | b | | | c | d |
| Pure_Ge | 1.5539 | 1.1520 | Ge_NW | 1 | - | - |
| Ge_shell_Si_core | 1.5539 | 1.1520 | Ge@Si_NW1 | 0.877 | 0 | 0.5918 |
| | | | Ge@Si_NW2 | 0.677 | 0.3840 | 0.8903 |
| | | | Ge@Si_NW3 | 0.385 | 0.7680 | 1.2369 |
| Si_shell_Ge_core | 1.5539 | 1.1520 | Si@Ge_NW1 | 0.615 | 0 | 0.5918 |
| | | | Si@Ge_NW2 | 0.323 | 0.3840 | 0.8903 |
| | | | Si@Ge_NW3 | 0.123 | 0.7680 | 1.2369 |
| Pure_Si | 1.5539 | 1.1520 | Si_NW | 0 | - | - |

The pair distribution function *g(r)* gives the probability of finding the atom pairs within a distance *r* in the system:

$$g(r) = \frac{1}{N^2}\langle \sum_i \sum_{j\neq 1} \delta(r - r_{ij})\rangle$$

10

where *N* is the number of atoms of the nanowires in simulation, and ⟨⟩ denotes the average value for the statistical time step.

All MD calculations were performed using the General Utility Lattice Program (GULP) package[34] with a time step of 1 fs throughout. All structures were thermalized from 300 K to 800K gradually at an increment of 50 K and were performed lattice energy minimization to find the lowest energy configuration through 1 000 000 time steps at each temperature. Then, the relaxed structures were simulated to get mechanical properties. The initial structures for each temperature are from the coordinates of the last time step of the previous temperature.

In the tensile simulation process, the nanowires were stretched along the axial direction. The strain rate is selected to perform tensile simulations with a tensile strain of 0.005 applied each time during the stretching process, and this process is repeated until the nanowires are broken.

The potential energy $E_{av}$ per atom at each temperature is defined below,

$$E_{av} = \frac{1}{N} < E_{tot} >$$

11

The local stress tensors $\sigma_i$ of each atom *i* is given in the following equation:

$$\sigma_i^{ab} = \frac{1}{V_i} \sum_{j \neq i} \frac{\partial E_i}{\partial r_{ij}} \frac{r_{ij}^a r_{ij}^b}{r_{ij}}$$

12

where $V_i$ is the volume of atoms, $E_i$ is the energy of the *i* th atom and $r_{ij}^a$ and $r_{ij}^b$ are the Cartesian components of the vector $r_{ij}$ in which *a, b* stand for *x, y, z*. Furthermore, the isotropic pressure $P_i$ on the atom is related to the $\sigma_i$ as given by the following form:

$$P_i = \frac{1}{3}(\sigma_i^{xx} + \sigma_i^{yy} + \sigma_i^{zz})$$

13

The heat capacity at a certain temperature *T*, is given by the following formula

$$Cv = \int_0^{\omega_m} k_B g(\omega) \frac{\left( \hbar \omega / k_B T \right)^2 e^{\hbar \omega / k_B T}}{\left( e^{\hbar \omega / k_B T} - 1 \right)^2} d\omega$$

14

where $g(\omega)$ represents the density of the angular frequency ω, $\omega_m$the maximum angular frequency, ħ the Planck Constant, and $k_B$ Boltzmann Constant.

# 3 Results And Discussion

Ge@Si and Si@Ge nanowires with different core-shell ratios.

Figure 2 shows variation of the average energy per atom with the temperatures on heating. By comparing the average energy curves of pure Si, pure Ge and six core@shell nanowires, it can be seen from the figure that the average energy increases in a linear mode with the increase of the temperatures, which is caused by the gradually intensification of the thermal vibrations of the atoms around their lattice positions with increasing the temperature. Here, the atoms in these nanowires can hold their packing patterns in the temperature ranges. In meanwhile, as the germanium content increases, the average energy increases.

In order to understand the structural characteristics of Ge@Si and Si@Ge nanowires, the PDFs are shown in Fig. 3, that there are discrete peaks with a certain width due to the thermal movement of atoms around their equilibrium position. Here, for the pure Ge and Si nanowires, the locations of the first peaks are at about 0.245 nm and 0.236 nm, respectively, while those of the core@shell nanowires are located between them. The location of one peak corresponds to the distance between paired atoms, and these distinct peaks indicate orderly packing patterns. It should be noted that the height of the first peak of the PDFs for these core@shell nanowires decrease compared with those of pure Si and Ge nanowires, and it is obvious that the thicker the shell, the higher the height of the peak, especially at relatively low temperatures. It is because the thicker the shell, the less Si-Ge atomic pairs and the more Si-Si or Ge-Ge atomic pairs, suggesting that the component content plays a significant role in different nanowires. In addition, for Si@Ge_NW1, there is an apparent splitting phenomenon when the distance exceeds the second neighbor distances. When the temperature increases, the shapes of these discrete peaks become passivated, the height of the peaks decreases and the width increases overall owing to intensified thermal vibration.

Figure 4 shows the stress–strain relationship for the tensile process of the Ge@Si and Si@Ge nanowires with different core-shell ratios at different temperatures. As shown in this figure, all the nanowires start with a linear relationship between stress value and small strain at room temperature, indicating that these nanowires undergo elastic deformation following the Hook's law. The slope of the stress–strain curve near zero strain gives the Young's modulus. At small strains, the distribution of the pressure on each atom is calculated and the result as shown in the following Fig. 7, where the atoms are under positive and negative pressure. It is worth noting that the value of the stress for the pure Ge nanowire is significantly higher than that of core/shell nanowires with silicon cores. The stress value of the pure Si nanowire is also higher than that of the corresponding Ge as core filled core/shell nanowires. Under stretching, the slope of curves gradually decreases, and the stress-strain of nanowires no longer follows a linear relationship, where some of these wires apparently enter into the yielding state at this time. As shown in Fig. 5, atomic packing images of the typical structures show that some of the surface atoms leave their origin lattice positions, resulting in some lattice defects, while most of the inner atoms still are at lattice positions. In the meantime, the length between the wires is obviously elongated. In these curves, there is an obvious yielding stage for the pure Ge_NW or Si@Ge_$NW_2$. For the pure Ge_NW, as the strain increases to 0.2, the atoms are significantly stretched along the [-1 0 0] direction. When the strain exceeds 0.2, the lattice still continues to be elongated and the stress drops slightly to 6.364 GPa at this time, corresponding to the yield strength. Similarly, this phenomenon also appears on Si@Ge_$NW_2$, and the corresponding yield strength is 5.184 GPa when the strain reaches 0.14. For the stress of these nanowires reaching a maximum or the tensile strength (*Rm*), the corresponding strain is written as $\varepsilon_{max}$. It can be seen in Fig. 5 that the atomic packing of these nanowires appears to be disorder at the moment, resulting in a large number of defects in them. In Fig. 7, it can be seen that only a small number of the atoms is under negative pressure. Then, there is an abrupt drop in stress. The atomic packing images show that a necking phenomenon occurs in these nanowires, as shown in Fig. 5. As depicted in Fig. 4**(b)**, the stress-strain curves at 800K have no obvious elastic stage. From the perspective of lattice vibration, as the temperature increases, the thermal motion of the atoms is more intense, which generates greater

amplitude from its equilibrium position. Under external loads, the atoms can be away from the equilibrium position easily, thus the stress increases nonlinearly with the strain.

The atomic packing of some typical nanowires is shown in Fig. 5. At a small strain, the distance between the atoms increases slightly, and only some of the atoms in shell surface are rearranged, resulting in some local lattice defects while most of the atoms are still at the lattice positions. Under stretching, the atoms inside the nanowires are also rearranged, and the defects increase. Then, as the strain further increases, the defects expand from the middle part to both sides of the nanowires until the necking phenomena occurs.

with different core-shell ratios at 300 K.

It can be seen from the stress-strain curves in Fig. 4 that when the temperature reaches 800K, there is no obvious elastic stage, so only the Young's modulus of different Ge@Si and Si@Ge nanowires at 300K is illustrated in Fig. 6. It can be apparently seen that the Young’s modulus of the Ge@Si nanowires decrease compared to those of the pure Ge nanowires, whereas the Young’s modulus of the Si@Ge nanowires increase compared to the pure Si ones. As the Ge content decreases, the value of the Young's modulus of the Ge@Si nanowires increases significantly. However, with the Ge content changed in Si@Ge nanowires, there is only small influence in the Young’s modulus of these nanowires.

**Table 3** lists the tensile strengths of all nanowires, that the tensile strengths decrease as the temperature increases. As far as known, the higher temperature is, the more easily the atoms escape from their equilibrium position, resulting in lattice defects. At the same strain, the lattice defects of the nanowires are more intense at higher temperature so that the nanowires are more easily to reach their tensile limits. Therefore, the tensile strengths of the nanowires at 800 K will be lower than those at 300 K. Compared with the pure Ge nanowire, it can be observed that the elongations of the Ge@Si nanowires increased, but the tensile strength decreased. Moreover, as the silicon content increases, the elongation and tensile strength decrease. At the same time, as the content of the silicon core increases, the nanowires will break prematurely. However, there is little decrease in tensile strengths of the Si@Ge nanowires compared to those of the pure Si nanowire.

**Table 3.** Tensile Strength of Ge@Si and Si@Ge nanowires

with different core-shell ratios at 300 K and 800 K.

| Label | 300 K | | 800 K | |
|---|---|---|---|---|
| | Strain | Tensile Strength (*Rm* /GPa) | Strain | Tensile Strength (*Rm*/GPa) |
| Ge_NW | 0.32 | 7.73736 | 0.24 | 6.9425 |
| Ge@Si_NW1 | 0.38 | 7.49919 | 0.28 | 6.86628 |
| Ge@Si_NW2 | 0.36 | 6.36021 | 0.28 | 6.35699 |
| Ge@Si_NW3 | 0.34 | 5.91928 | 0.26 | 5.13656 |
| Si@Ge_NW1 | 0.36 | 6.09235 | 0.3 | 5.93173 |
| Si@Ge_NW2 | 0.34 | 5.9722 | 0.26 | 5.7421 |
| Si@Ge_NW3 | 0.34 | 6.29431 | 0.26 | 5.86117 |
| Si_NW | 0.34 | 6.411 | 0.24 | 6.09667 |

Figure 7 shows the isotropic pressure distributions of these nanowires with different core-shell ratios at a small strain and $\varepsilon_{max}$ corresponding to the yield state during stretching processes. It can be seen that the pressure distributions trend at 300 K and 800 K is similar. At the small strain, the pressures on the atoms are distributed around zero and the atoms are subjected to positive and negative pressure, indicating that most of the atoms are less stressed, and the pressures distributions are more concentrated. When the strain reaches their tensile strengths, the pressure increases significantly and most of the atoms have a positive pressure. As the strain increases, the pressures distributions become wider, indicating that the disorder degree of the atoms increases. It should be noted that when the strain is small, the range of the pressure distribution of the Si@Ge_NW2 at 800K significantly larger than that of the other nanowires because the Si@Ge_NW2 has more lattice defects as mentioned above.

As shown in Fig. 8 for these core-shell nanowires, compared to the pure Ge nanowire, the peak at around 120 $cm^{-1}$ gradually becomes wider and shifts to high frequencies by introducing Si atoms, and finally the transverse acoustic (TA) mode of the pure silicon nanowire occurs in region #1. In meanwhile, the longitudinal acoustic (LA) mode of Ge at around 200 $cm^{-1}$ is also shifted from the pure Ge nanowires mode toward that pure Si nanowires mode. The longitudinal optical (LO) mode at around 300 $cm^{-1}$ shifts to high frequency and the peak value decreases in region #2, which eventually form the longitudinal acoustic (LA) mode of the Si nanowire accompanied with the increase of the peak at 480 $cm^{-1}$ in region #3. For the Si@Ge nanowires, while introducing the Ge atoms into pure the Si nanowire, the presence of the Ge atoms splits the peak at around 180 $cm^{-1}$ and gradually shifts to the low frequencies, eventually forming the TA and LA modes of the pure Ge nanowire in region #1. Then with the increase of Ge concentration, the height of the peak at around 480 $cm^{-1}$ decreases in region #3 and shifts to the low frequencies. Eventually, the longitudinal optical (LO) mode of the pure Ge nanowire in region #2 occurs together with the increase of the peak height at 300 $cm^{-1}$. In addition, with the increase of strain, the

optical phonon modes at high frequency shift towards the low frequency positions, indicating the occurrence of the phenomenon named as ‘phonon softening’. Here, compared with unstrained state, most of phonons having high frequencies will have a lower energy under tension. This is due to the fact that with the increase of the strain, the elasticity recovery force becomes weaken, resulting in the frequency shift of the optical mode to the low values.

Figure 9 shows that the heat capacity of the nanowires with different core-shell ratios at strains of 0, 0.005 and 0.015. As shown in this Fig. 9, the heat capacities of the unstained Si and Ge nanowires are 41051 $J{\cdot}mol^{-1}{\cdot}K^{-1}$ and 47359 $J{\cdot}mol^{-1}{\cdot}K^{-1}$ respectively, which is slightly higher than those of the bulk Si and Ge[35] due to the phonon’s confinement effect in the nanowires. As the Si or Ge content changes, the heat capacities of the core-shell nanowires are between the heat capacity values of the pure Si and Ge nanowires. Moreover, because the phonon modes shift towards low frequencies with decreasing the Ge content, the heat capacity of both the Ge@Si and Si@Ge nanowires decrease. It is also noting that the Ge@Si and Si@Ge nanowires with similar contents have similar heat capacities. Then, compared to the unstrained conditions, because of applying the strain, the energy corresponding to the vibrations decreases in the optical phonon modes decrease, resulting in the increases of the heat capacities of these nanowires.

# 4 Conclusion

In this work, the structure, atomic level stress and mechanical properties as well as thermal properties for the Ge@Si and Si@Ge core–shell nanowires having different core-shell ratios with the wire axis in the [110] direction, have been studied using molecular dynamics within the formalism of Tersoff potential. Through the tensile simulations at different temperatures, the nanowires present elastic deformation, yield, strain strengthening, and necking at room temperature. However, there is no obvious elastic stage for all the nanowires at 800 K. Furthermore, the Young’s modulus of the Ge@Si nanowires is decreased compared with pure Ge nanowires, whereas the modulus of the Si@Ge nanowires has increased compared with pure Si nanowires. Compared with pure Ge nanowire, it can be apparently seen that the elongations of the Ge@Si nanowires increased, but the tensile strength decreased. In addition, as the silicon content increases, the elongation and tensile strength decrease. Finally, it is found that the pressures on the atoms at a small strain are small and most of them are subjected to positive and negative pressure. However, while the strain reaches their respectively tensile strength, the pressure increases significantly and most of the atoms undergo apparently positive pressure. In addition, the atomic level pressures of these nanowires present differences under tension indicating the differences of the atomic packing in them. The vibrational modes including forming, expanding, shifting, degenerating, and disappearing are characterized from the phonon’s DOS. At room temperature, the Ge concentration in the nanowires greatly affects the heat capacities of the nanowires.

# Declarations


### ACKNOWLEDGMENTS

Project supported by the National Natural Science Foundation of China (Grant No. 51671051)

### DATA AVAILABILITY

The datasets used and/or analyzed during the current study are available from the corresponding author on reasonable request.

# References


1. 1. Dresselhaus, M. S. *et al.* New Directions for Low-Dimensional Thermoelectric Materials. *Adv. Mater.* **19**, 1043–1053 (2007).
2. 2. Mauser, K. W. *et al.* Employing Cathodoluminescence for Nanothermometry and Thermal Transport Measurements in Semiconductor Nanowires. *ACS Nano* **15**, 11385–11395 (2021).
3. 3. Lim, B., Cui, X. Y. & Ringer, S. P. Strain-mediated bandgap engineering of straight and bent semiconductor nanowires. *Phys. Chem. Chem. Phys.* **23**, 5407–5414 (2021).
4. 4. Li, J.-F., Liu, W.-S., Zhao, L.-D. & Zhou, M. High-performance nanostructured thermoelectric materials. *NPG Asia Mater.* **2**, 152–158 (2010).
5. 5. Vineis, C. J., Shakouri, A., Majumdar, A. & Kanatzidis, M. G. Nanostructured Thermoelectrics: Big Efficiency Gains from Small Features. *Adv. Mater.* **22**, 3970–3980 (2010).
6. 6. Wu, Y., Fan, R. & Yang, P. Block-by-Block Growth of Single-Crystalline Si/SiGe Superlattice Nanowires. *Nano Lett.* **2**, 83–86 (2002).
7. 7. Shimizu, T., Zhang, Z., Shingubara, S. & Senz, S. Vertical Epitaxial Wire-on-Wire Growth of Ge/Si on Si(100) Substrate. *Nano Lett* **9**, 4 (2009).
8. 8. Dayeh, S. A. *et al.* Growth, Defect Formation, and Morphology Control of GermaniumÀSilicon Semiconductor Nanowire Heterostructures. *Nano Lett.* 7 (2011).
9. 9. Varahramyan, K. M., Ferrer, D., Tutuc, E. & Banerjee, S. K. Band engineered epitaxial Ge–SixGe1 – x core-shell nanowire heterostructures. *Appl. Phys. Lett.* **95**, 033101 (2009).
10. 10. Lauhon, L. J., Gudiksen, M. S., Wang, D. & Lieber, C. M. Epitaxial core–shell and core–multishell nanowire heterostructures. *Nature* **420**, 57–61 (2002).
11. 11. Bi, K. *et al.* The thermal conductivity of SiGe heterostructure nanowires with different cores and shells. *Phys. Lett. A* **376**, 2668–2671 (2012).
12. 12. Xie, G. *et al.* Ultralow thermal conductivity in Si/Ge $_{x}$ Si $_{1-x}$ core-shell nanowires. *J. Appl. Phys.* **113**, 083501 (2013).
13. 13. Hu, M., Giapis, K. P., Goicochea, J. V., Zhang, X. & Poulikakos, D. Significant Reduction of Thermal Conductivity in Si/Ge Core – Shell Nanowires. *Nano Lett.* **11**, 618–623 (2011).
14. 14. Wang, S., Shan, Z. & Huang, H. The Mechanical Properties of Nanowires. *Adv. Sci.* **4**, 1600332 (2017).

15. 15. Jing, Y. & Meng, Q. Molecular dynamics simulations of the mechanical properties of crystalline/amorphous silicon core/shell nanowires. *Phys. B Condens. Matter* **405**, 2413–2417 (2010).
16. 16. Sarkar, J. Investigation of mechanical properties and deformation behavior of single-crystal Al-Cu core-shell nanowire generated using non-equilibrium molecular dynamics simulation. *J. Nanoparticle Res.* **20**, 153 (2018).
17. 17. Sarkar, J. & Das, D. K. Molecular dynamics study of defect and dislocation behaviors during tensile deformation of copper-silver core-shell nanowires with varying core diameter and shell thickness. *J. Nanoparticle Res.* **20**, 272 (2018).
18. 18. Liu, X. W., Hu, J. & Pan, B. C. The composition-dependent mechanical properties of Ge/Si core–shell nanowires. *Phys. E Low-Dimens. Syst. Nanostructures* **40**, 3042–3048 (2008).
19. 19. Thanh, V., Quang, T., Hung, N., Vu, H. & Truong, D. Investigate the mechanical properties of Si/Ge (Ge/Si) core-shell nanowires: A molecular dynamics study. *Sci. Technol. Dev. J. - Eng. Technol.* **3**, first (2020).
20. 20. Zhu, Y. *et al.* First-principles investigations on thermodynamic properties of the ordered and disordered Si0.5Ge0.5 alloys. *Appl. Phys. A* **115**, 667–670 (2014).
21. 21. Zhang, Y., Cao, J. X., Xiao, Y. & Yan, X. H. Phonon spectrum and specific heat of silicon nanowires. *J. Appl. Phys.* **102**, 104303 (2007).
22. 22. Xu, Y. & Li, G. Strain effect analysis on phonon thermal conductivity of two-dimensional nanocomposites. *J. Appl. Phys.* **106**, 114302 (2009).
23. 23. Meyer, R. *et al.* Changes in the phonon density of states of Fe induced by external strain. *Appl. Phys. A* **127**, 5 (2021).
24. 24. Pili, L. *et al.* Dynamics and thermodynamics of a topological transition in spin ice materials under strain. *ArXiv210507977 Cond-Mat* (2021).
25. 25. Algharagholy, L. A. A., Pope, T. & Lambert, C. J. Strain-induced bi-thermoelectricity in tapered carbon nanotubes. *J. Phys. Condens. Matter* **30**, 105304 (2018).
26. 26. Kuang, Y. D., Lindsay, L., Shi, S. Q. & Zheng, G. P. Tensile strains give rise to strong size effects for thermal conductivities of silicene, germanene and stanene. *Nanoscale* **8**, 3760–3767 (2016).
27. 27. Hunt, M. *et al.* Ultimate Tensile Strengths of 3D Printed Carbon-fiber Reinforced Thermoplastics in Liquid Nitrogen. *IOP Conf. Ser. Mater. Sci. Eng.* **755**, 012118 (2020).
28. 28. Tersoff, J. Modeling solid-state chemistry: Interatomic potentials for multicomponent systems. *Phys. Rev. B* **39**, 5566–5568 (1989).
29. 29. Haskins, J. B., Kinaci, A. & Çağin, T. Thermal conductivity of Si–Ge quantum dot superlattices. *Nanotechnology* **22**, 155701 (2011).
30. 30. Aryal, S., Paudyal, D. & Pati, R. Cr-Doped Ge-Core/Si-Shell Nanowire: An Antiferromagnetic Semiconductor. *Nano Lett.* **21**, 1856–1862 (2021).

31. 31. Xiang, J. *et al.* Ge/Si nanowire heterostructures as high-performance field-effect transistors. *Nature* **441**, 489–493 (2006).
32. 32. Aryal, S. & Pati, R. Spin filtering with Mn-doped Ge-core/Si-shell nanowires. *Nanoscale Adv.* **2**, 1843–1849 (2020).
33. 33. Stukowski, A. Visualization and analysis of atomistic simulation data with OVITO–the Open Visualization Tool. *Model. Simul. Mater. Sci. Eng.* **18**, 015012 (2009).
34. 34. Gale, J. D. & Rohl, A. L. The General Utility Lattice Program (GULP). *Mol. Simul.* **29**, 291–341 (2003).
35. 35. Flubacher, P., Leadbetter, A. J. & Morrison, J. A. The heat capacity of pure silicon and germanium and properties of their vibrational frequency spectra. *Philos. Mag.* **4**, 273–294 (1959).

# Figures

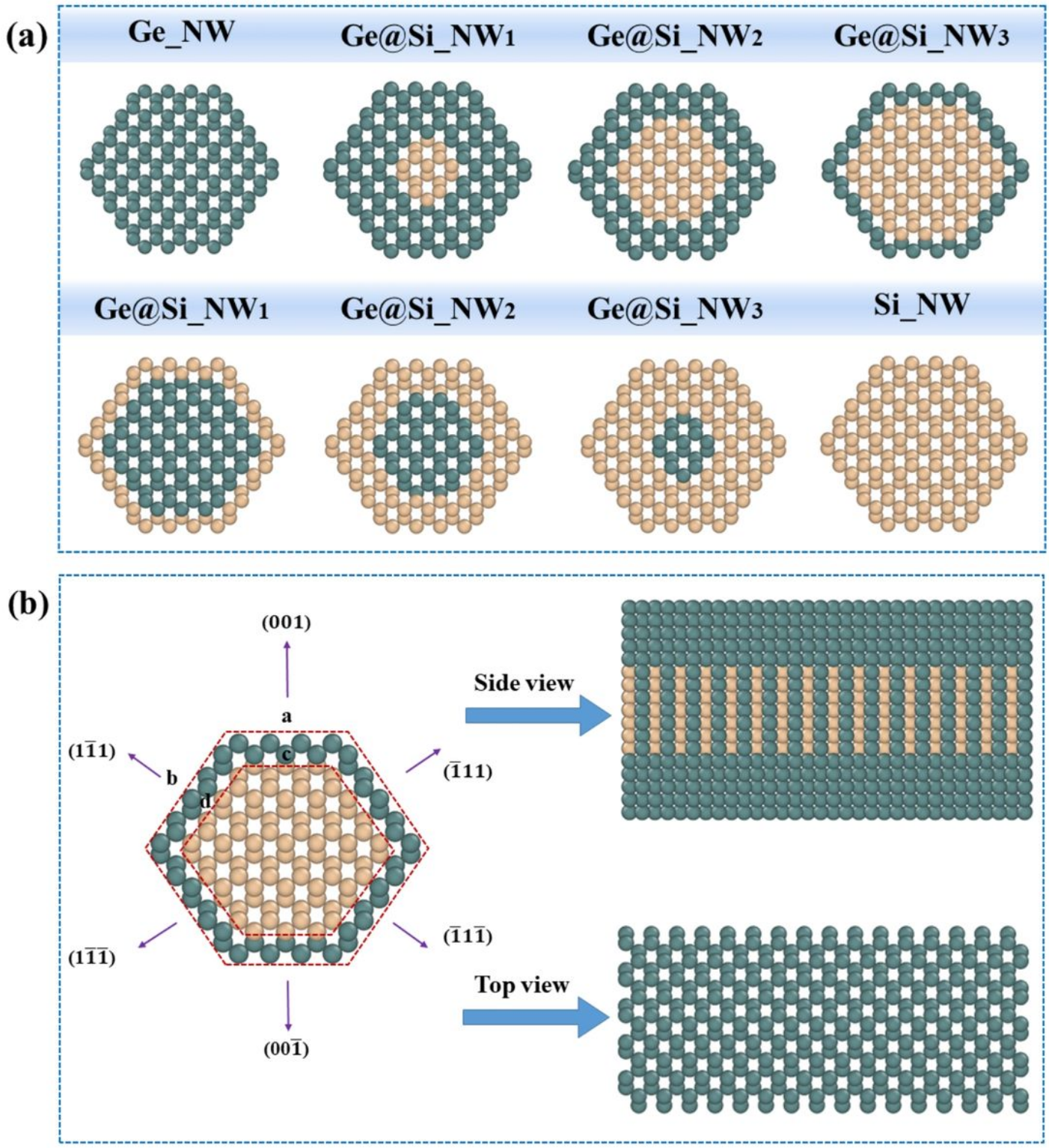


## Figure 1

(a)Two-dimensional projection of atomic structures of initial cross section for Ge@Si and Si@Ge nanowires from [110]-oriented view; (b) the typically example of two-dimensional projection of atomic structures of all view for Ge@Si_NW3.

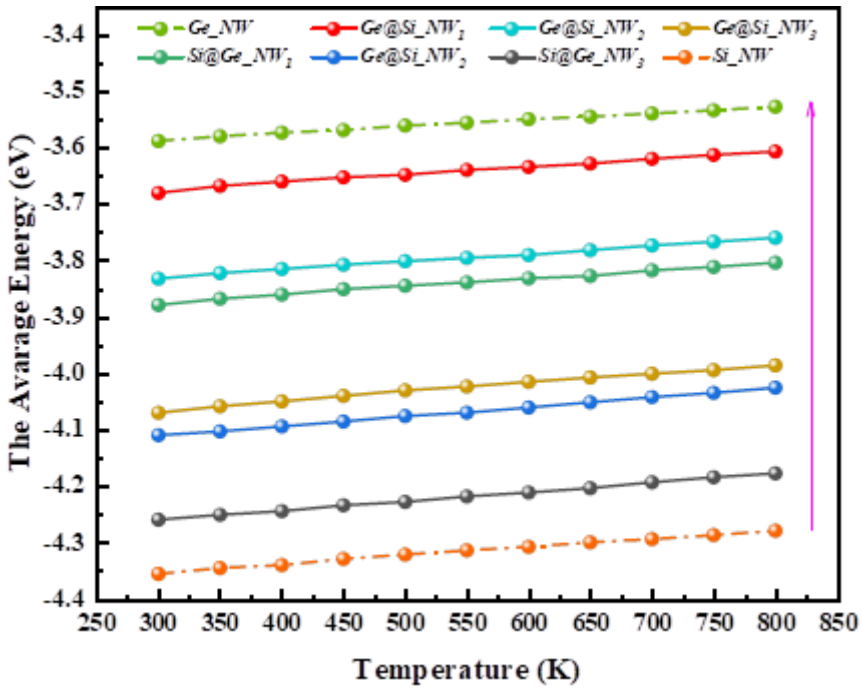


## Figure 2

Variation of potential energy per atom of

Ge@Si and Si@Ge nanowires with different core-shell ratios.

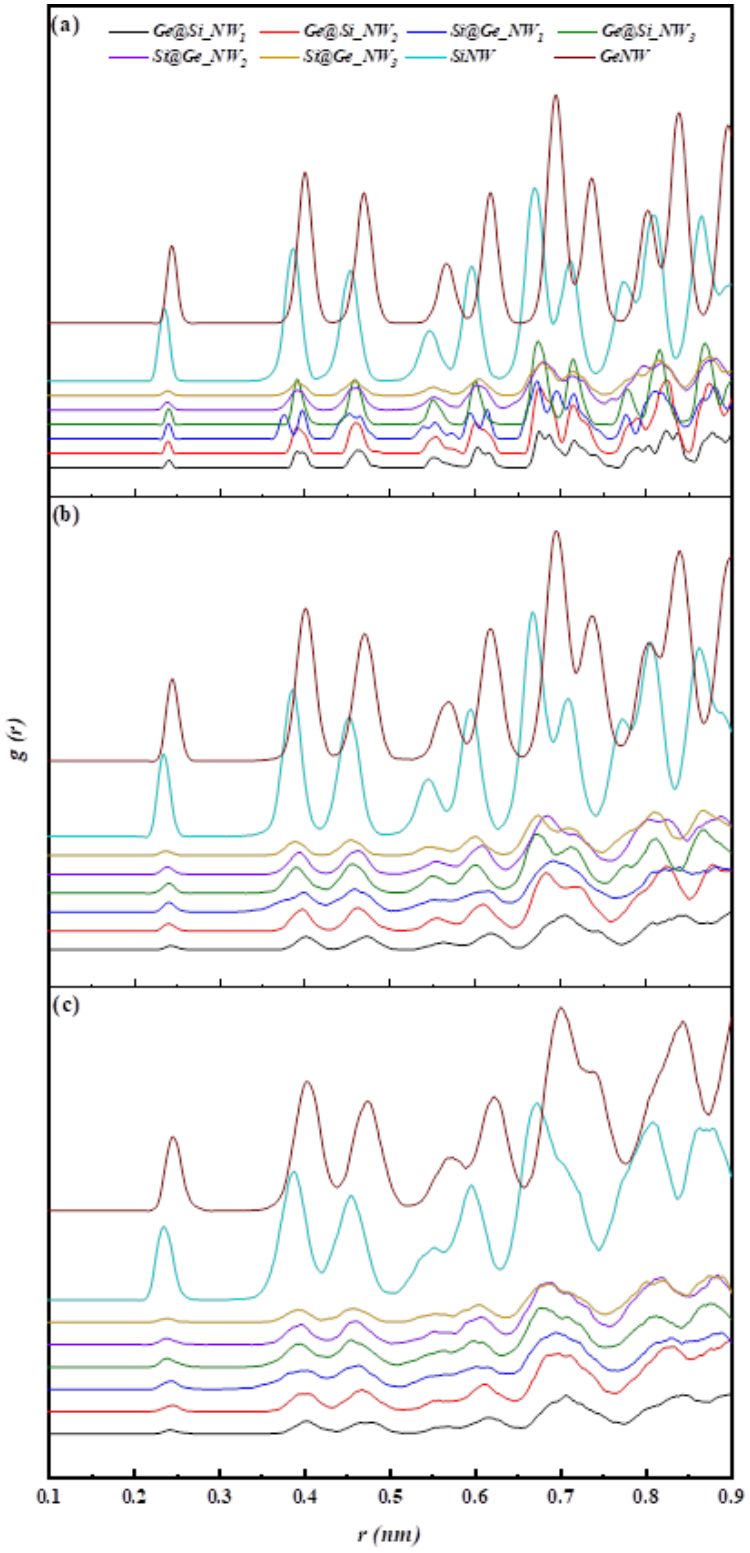


## Figure 3

The PDFs of *Ge@Si* and *Si@Ge* nanowires with different core-shell ratios after structural relaxation at different temperature (a)300 K; (b)450 K; (c)800 K.

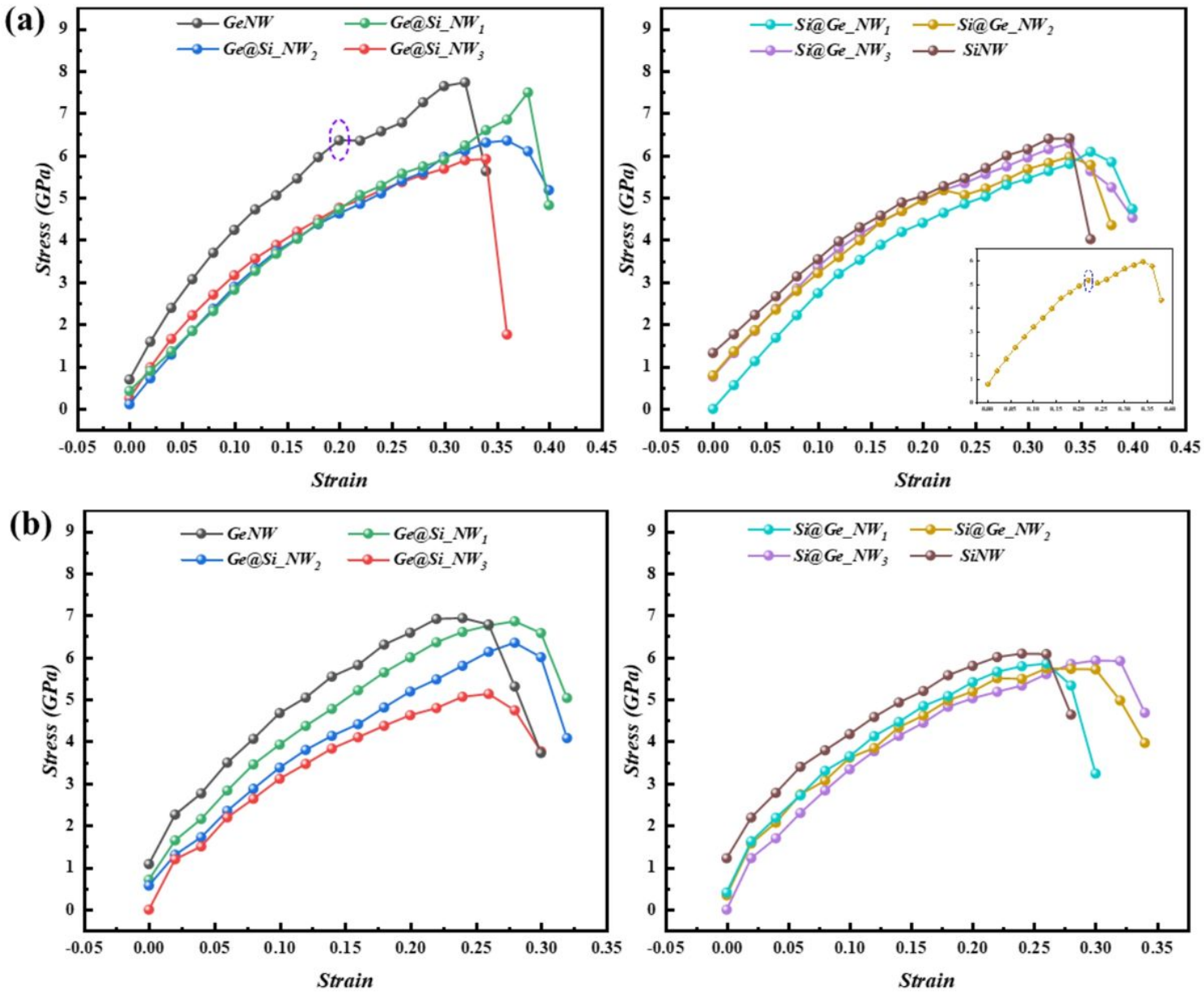


## Figure 4

Stress-strain curves of Ge@Si (Left) and Si@Ge (Right) nanowires with different core-shell ratios at different temperatures:(a) 300 K; (b) 800 K.

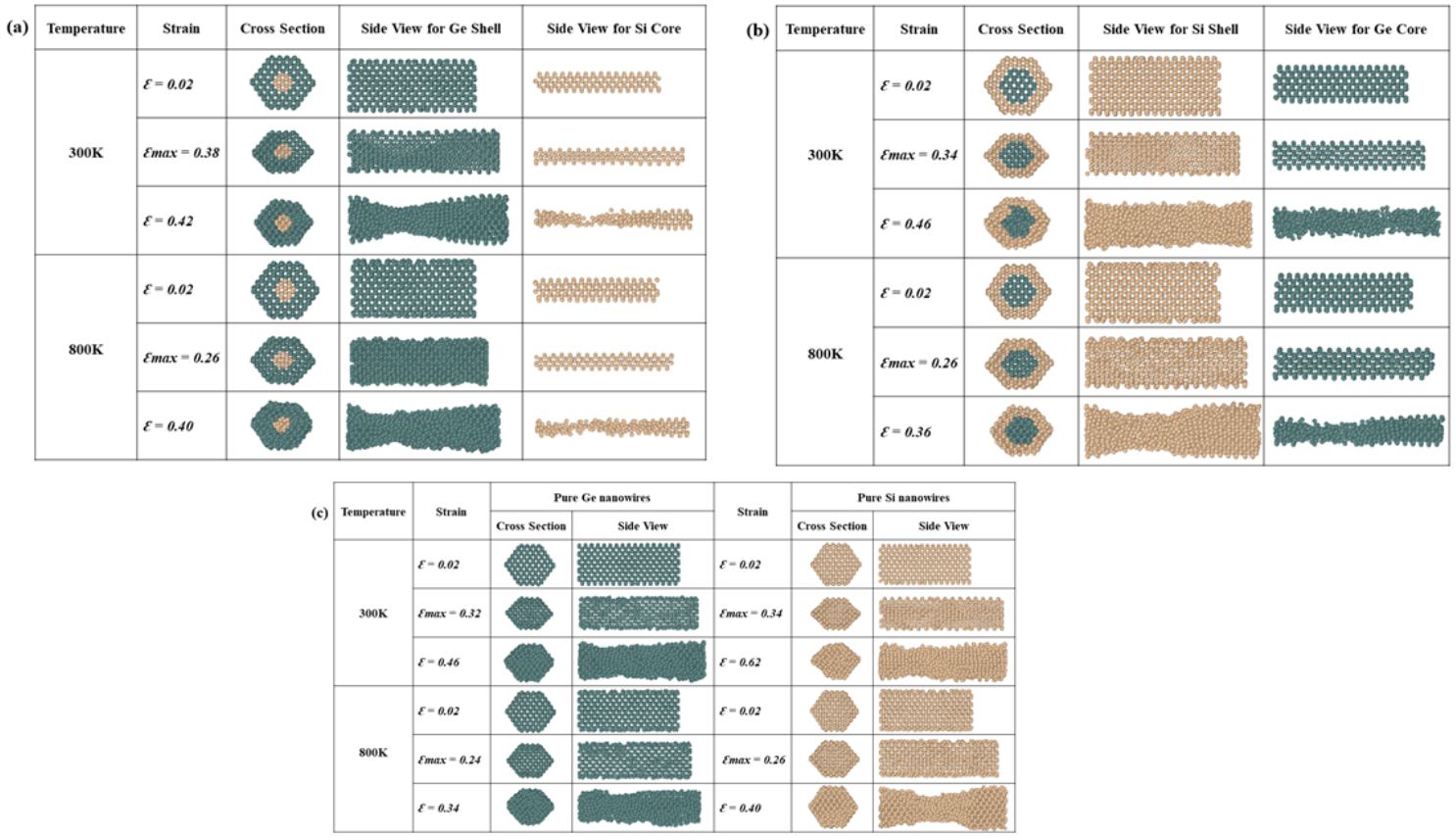


## Figure 5

The evolutionary morphologies of different nanowires at different temperatures during stretching processes: (a)the packing structure of Ge@Si_NW1 at 300 K and 800 K; (b)the packing structure of Si@Ge_NW2 at 300 K and 800 K; (c)the packing structure of pure Ge_NW and Si_NW at 300 K and 800 K.

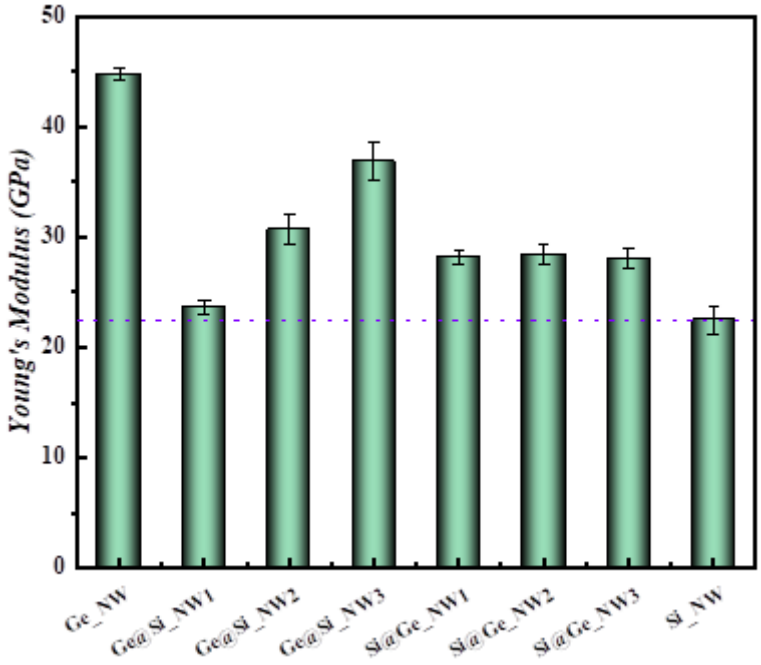


**Figure 6**

Young's modulus of Ge@Si and Si@Ge nanowires with different core-shell ratios at 300 K.

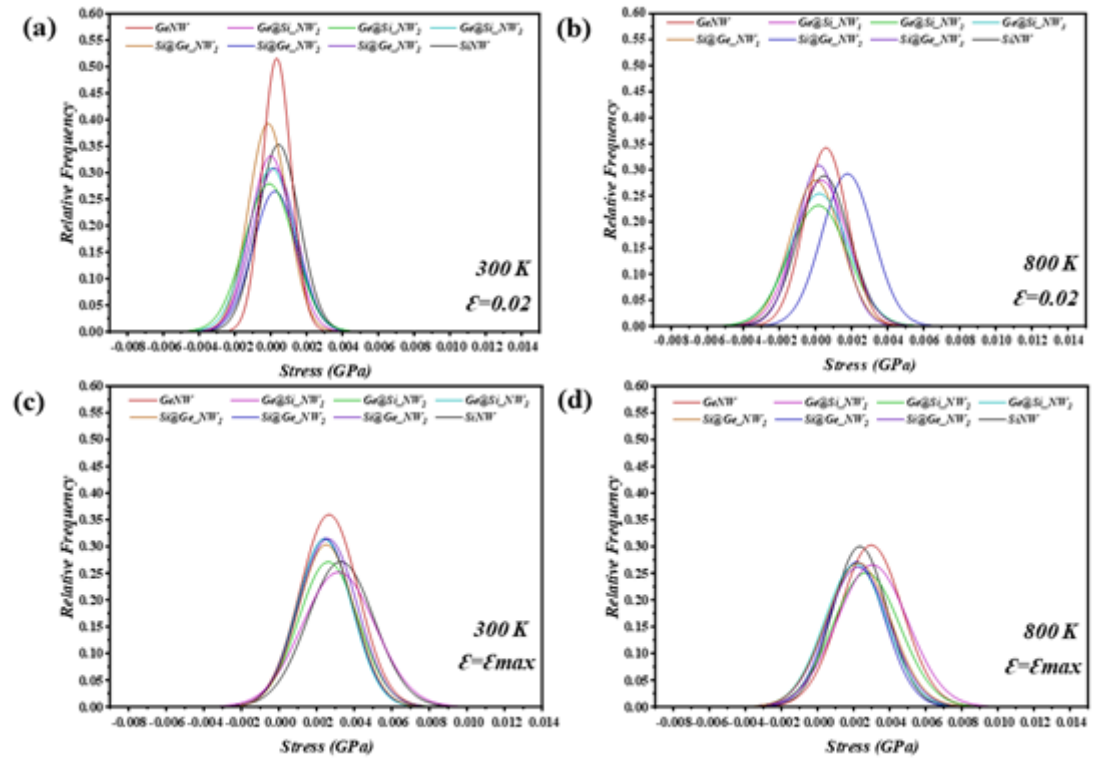


**Figure 7**

Pressure distributions on the atoms for the Ge@Si and Si@Ge nanowires with different core-shell ratios at different temperatures during stretching processes: (a) 300 K and the strain is 0.02; (b) 800 K and the strain is 0.02; (c) 300 K and the strain is $\varepsilon_{max}$; (d) 800 K and the strain is $\varepsilon_{max}$.

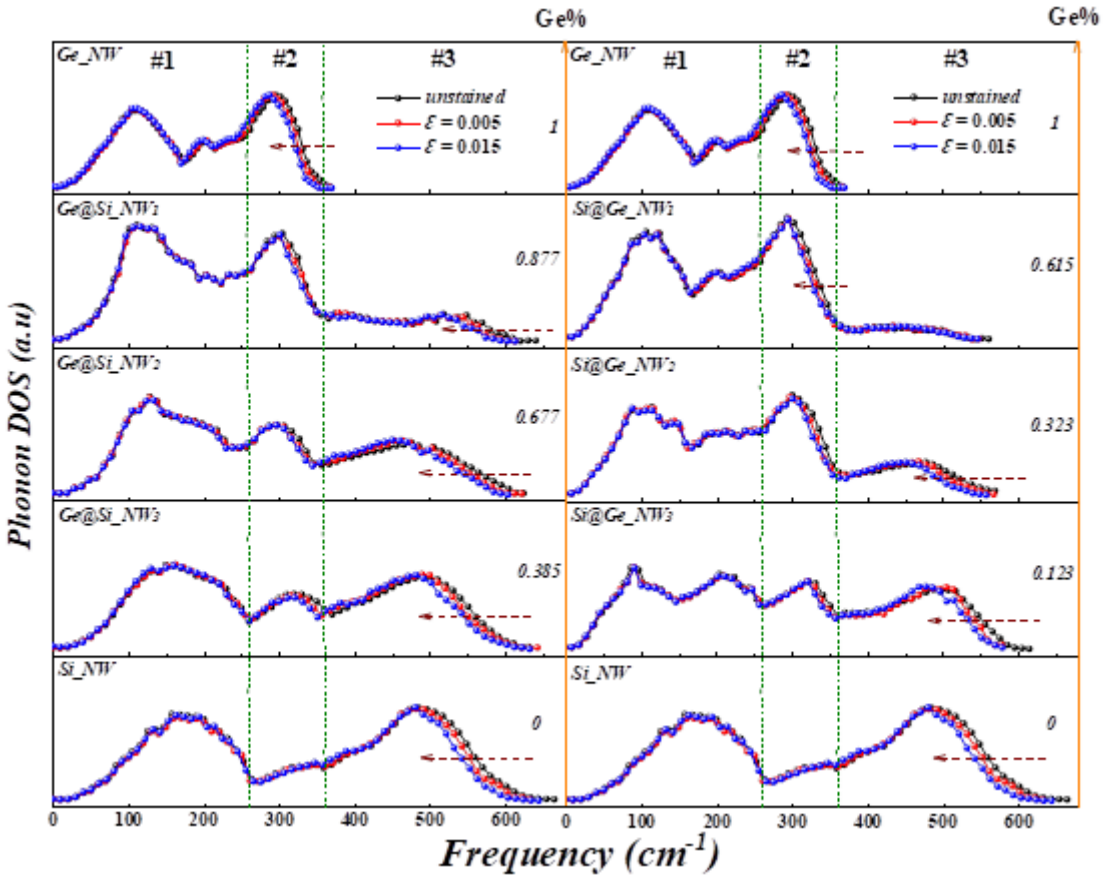


## Figure 8

Phonon Density of State (PDOS) of Ge@Si and Si@Ge nanowires with different core-shell ratios at 300 K.

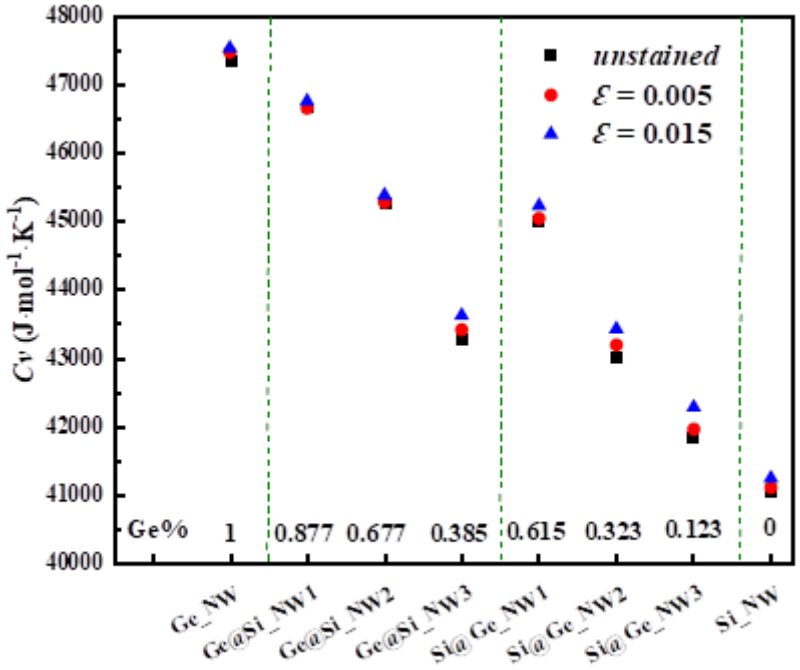


## Figure 9

Heat capacity (Cv) of Ge@Si and Si@Ge nanowires with different core-shell ratios at 300 K: (a) Ge@Si; (b) Si@Ge.